ACS APPLIED MATERIALS & INTERFACES

www.acsami.org

Research Article

Enhanced Electrocatalytic Oxidation of Small Organic Molecules on Platinum-Gold Nanowires: Influence of the Surface Structure and Pt-Pt/Pt-Au Pair Site Density

Nicole Smina, Adam Rosen, Lukasz Sztaberek, William Beatrez, Kathryn Kingsbury, Rosario Troia, Yongchen Wang, Jing Zhao, Joshua Schrier,* and Christopher Koenigsmann*

Cite This: *ACS Appl. Mater. Interfaces* 2021, 13, 59892–59903

Read Online

ACCESS | Metrics & More | Article Recommendations | Supporting Information

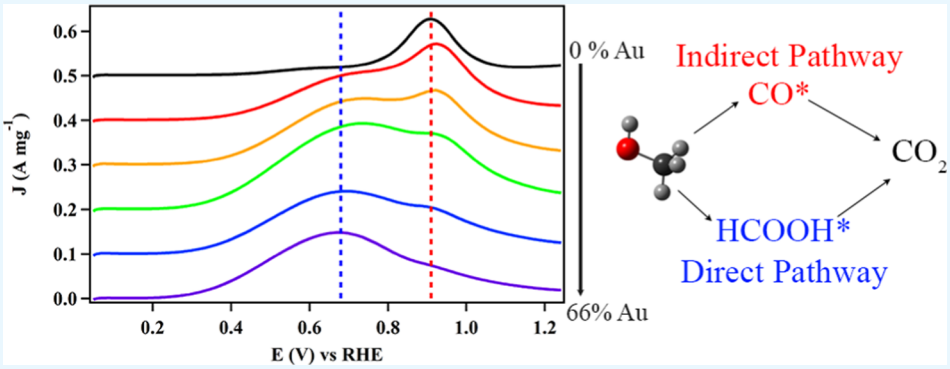

ABSTRACT: The electrochemical oxidation of small organic molecules (SOMs) such as methanol and glucose is a critical process and has relevant applications in fuel cells and sensors. A key challenge in SOM oxidation is the poisoning of the surface by carbon monoxide (CO) and other partially oxidized intermediates, which is attributed to the presence of Pt−Pt pair sites. A promising pathway for overcoming this challenge is to develop catalysts that selectively oxidize SOMs via "direct" pathways that do not form CO as a primary intermediate. In this report, we utilize an ambient, template-based approach to prepare PtAu alloy nanowires with tunable compositions. X-ray photoelectron spectroscopy measurements reveal that the surface composition matches that of the bulk composition after synthesis. Monte Carlo method simulations of the surface structure of PtAu alloys with varying coverage of oxygen adsorbates and varying degrees of oxygen adsorption strength reveal that oxygen adsorption under electrochemical conditions enriches the surface with Pt and a large fraction of Pt−Pt sites remain on the surface even with the Au content of up to 50%. Electrochemical properties and the catalytic performance measurements of the PtAu nanowires for the oxidation of methanol and glucose reveal that the mechanistic pathways that produce CO are suppressed by the addition of relatively small quantities of Au (~10%), and CO formation can be completely suppressed by 50% Au. The suppression of CO formation with small quantities of Au suggests that the presence of Pt−Au pair sites may be more important in determining the mechanism of SOM oxidation rather than Pt−Pt pair site density.

KEYWORDS: *methanol oxidation reaction, glucose oxidation reaction, formic acid oxidation, non-enzymatic glucose detection, Monte Carlo simulations, fuel cells, sensors*

INTRODUCTION

Nanostructured Pt is widely used as a catalyst for the oxidation of small organic molecules (SOMs) and has broad technological applications in catalysis, fuel cells, and sensors.[1−6] Platinum has several advantages in SOM oxidation such as a high catalytic activity and the ability to oxidize a wide range of functional groups including alcohols, carboxylic acids, aldehydes, and ketones. Considerable work has been dedicated to the oxidation of primary alcohols such as methanol and ethanol for the anode of direct alcohol fuel cells. Accordingly, the oxidation mechanism of methanol is well studied on Pt catalysts.[7−13] This has allowed for significant advances in catalyst activity, poisoning resistance, and long-term durability by tuning the morphology, size, composition, and, support material of the catalyst. For example, promising results have recently been achieved with thin-film catalysts based on

Received: September 7, 2021
Accepted: November 30, 2021
Published: December 10, 2021

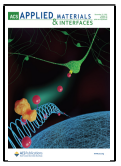

https://doi.org/10.1021/acsami.1c17244
ACS Appl. Mater. Interfaces 2021, 13, 59892−59903

atomically thin films of undercoordinated metal atoms.[14−19] Despite these advances, the oxidation mechanism for more complex SOMs containing a broader range of functional groups and carbon−carbon bonds is currently underway.

The mechanism of methanol oxidation on pure Pt follows an indirect pathway that leads to the production of adsorbed carbon monoxide (CO) as the primary intermediate.[20−24] The preferential formation of CO is believed to arise from Pt−Pt pair sites, which catalyze a rapid, multistep dehydrogenation of methanol at low overpotentials. Pt−Pt pair sites also bind strongly to the CO intermediate, leading to a high surface coverage at low overpotentials. Thus, the selective formation of the CO intermediate results in a poisoning effect because the oxidation of CO requires adsorbed oxygen species, which forms on the surface at relatively high overpotentials with respect to the thermodynamic potential for methanol oxidation. The poisoning effect of CO production in SOM oxidation is a key challenge in the oxidation of a wide range of SOMs including single and multicarbon substrates.

A common approach to overcoming the challenge of CO poisoning is to incorporate more oxophilic metals such as Ru into Pt alloys.[25−27] The oxophilic surface sites adsorb oxygen species at lower potentials than Pt and facilitate CO oxidation. This approach has been widely successful in increasing the activity and poisoning tolerance of Pt-based catalysts for the oxidation of methanol and formic acid. In addition, this strategy has also been used in Pt-based catalysts alloyed with Sn and Rh for ethanol oxidation, which not only increases CO tolerance but also facilitates the activation of the carbon−carbon bond.[28,29]

Alternatively, a second approach to reducing the effects of CO poisoning is to alloy Pt with other metals to reduce the density of Pt−Pt pair sites.[3] The density of Pt atoms at the surface and the density of Pt−Pt pair sites can be tuned by adjusting the relative Pt content of the alloy. Lowering the density of Pt−Pt pair sites decreases the binding strength of CO and slows the dehydrogenation steps, and thus, oxidation can proceed via a CO-free pathway.[30,31] For example, a prior work has shown that alloying Pt with first−row transition metals favors a direct, CO-free pathway for the oxidation of formic acid, which is a key intermediate in the oxidation of methanol.[32] Additionally, the density of Pt−Pt pair sites can also be tuned by alloying Pt with other precious metals that are less active toward SOM oxidation such as Au to promote a CO free pathway.[30,31,33−38] For example, Xing and co-workers found that PtAu alloys with Au occupying 60% of the surface sites maintain higher overall methanol oxidation activity and higher CO poisoning tolerance.[37] The enhancements in CO tolerance that arise from alloying Pt and Pd with less active metals have also been shown to increase the tolerance of precious metal-based catalysts toward the poisoning effects of fuel crossover in the cathode of direct alcohol fuel cells.[39−44]

Although the influence of pair site density on methanol oxidation has been investigated previously, the effect of Pt−Pt pair sites on the oxidation of more complex multicarbon substrates has not yet been systematically investigated. In this report, we investigate the influence of Pt−Pt pair site density on the oxidation of D-glucose. Glucose oxidation is an important electrochemical process for the detection of glucose via amperometric methods, and glucose can be utilized as a natural fuel source for implantable fuel cell devices in biomedical applications.[45−47] More importantly, the oxidation of glucose is more complex and involves breaking C−C bonds in addition to C−O and C−H bonds present in methanol. Thus, important new insights into the oxidation of SOMs can be gained by correlating the surface structure of Pt catalysts and the density of Pt−Pt pair sites.

A wide range of catalysts have been studied for glucose oxidation including precious metals such as Pt, Au, and Pd and first−row transitions metals such as Co and Ni.[45−57] Under acidic and neutral conditions, precious metal catalysts are more stable and active for glucose oxidation in comparison with first−row transition metals. The mechanism of D-glucose oxidation on Pt has been studied previously.[58−61] In acidic media, the oxidation of glucose on Pt-based catalysts occurs in a step-wise process and results in three oxidation waves on Pt(100) and on polycrystalline electrodes. The first oxidation wave (0.2−0.4 V) is attributed to the oxidation of the hemiacetal hydrogen on C1, leading to a gluconolactone intermediate. The second peak (0.7−0.9 V) is attributed to the oxidation of the carbon backbone of glucose and gluconolactone either adsorbed to the surface or present in the double layer leading to the formation of a range of oxidized carbon species including CO and CO_2. Although gluconolactone hydrolyzes to gluconic acid under acidic conditions, it is believed that the hydrolysis is slow relative to the electrochemical oxidation on the timescale of voltammetry. The final peak (1.0−1.2 V) occurs in the potential window where the surface of Pt is oxidized and the Pt−O* and Pt−OH* species may catalyze a further oxidation of the backbone to form CO and CO_2. However, the origin of the final peak remains a point of debate in the literature.[59] The oxidation mechanism has also been examined in neutral (physiological) pH and in basic conditions, which result in similar oxidation pathways on pure Pt catalysts.[60]

Although the mechanism has been studied on pure Pt, there are comparatively few reports devoted to bimetallic systems such as alloys and core−shell architectures.[57] In this report, we examine the influence of composition in $Pt_{1-x}Au_x$ alloy nanowires on the mechanism of methanol and glucose oxidation. Monodisperse PtAu alloy nanowires are prepared via an ambient, template-based approach that allows for direct control of composition by tuning the relative composition of Pt and Au precursors used in the reaction. We employ X-ray photoelectron spectroscopy (XPS) and Monte Carlo computational simulations to investigate the density of Pt sites on the surface of the alloy in vacuum and in an oxidizing electrolyte, respectively. Electrochemical measurements reveal that the tuning of the Au content has a significant impact on the catalytic properties of the catalyst and increasing the Au content suppresses pathways that generate CO in both methanol and glucose oxidation. Because CO is a poisoning intermediate in SOM oxidation, the use of PtAu alloys represents a promising approach to alleviating catalyst poisoning in the oxidation of both single and multi-carbon SOM substrates.

RESULTS AND DISCUSSION

The $Pt_{1-x}Au_x$ nanowires were synthesized via the ambient, template-based, double-diffusion method. Template-based methods are advantageous for synthesizing metallic electrocatalysts because they avoid the use of capping agents and surfactants, which strongly bind to the surface of the catalyst and block active sites. The *U*-tube (Figure S1) consists of two glass half-cells that are separated by a polycarbonate filter membrane. A precursor solution containing Pt and Au

https://doi.org/10.1021/acsami.1c17244
ACS Appl. Mater. Interfaces 2021, 13, 59892−59903

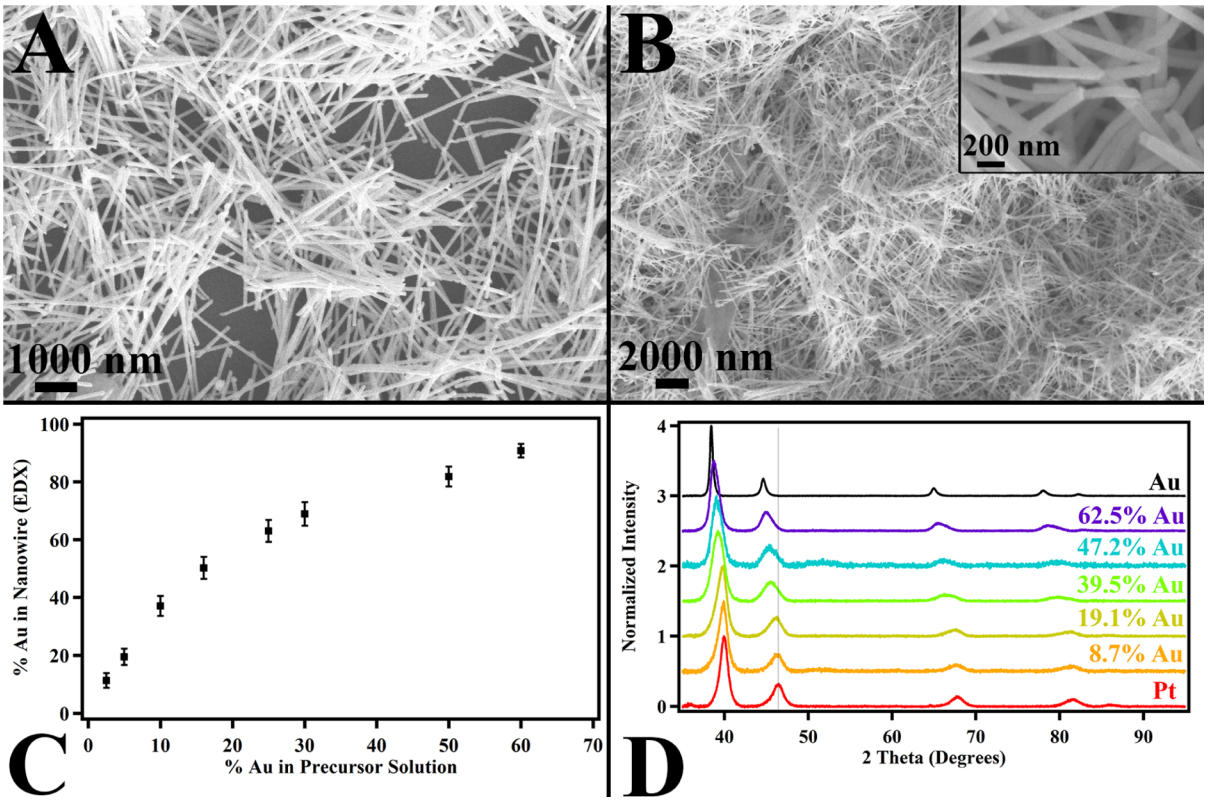

Figure 1. Characterization of the $Pt_{1-x}Au_x$ alloy nanowires. Scanning electron microscopy images of nanowires consisting of 10% (A) and 90% (B) gold. The inset is a high magnification image of the 90% Au nanowires highlighting the smooth surface texture of the wires. The composition of the nanowires measured by EDX spectroscopy is shown as a function of the composition of the precursor solution (C). Powder XRD patterns (D) collected from nanowire samples with compositions ranging from 0 to 100% gold. The vertical line denotes the position of the (200) peak of the pure platinum nanowires.

precursors is loaded in one half-cell, and a reducing agent solution is loaded in the other. The precursor and reducing agent solutions diffuse into the tubular pores of the polycarbonate membrane resulting in the reduction of the precursor. The nucleation and growth of the metal is directed by the size and shape of the tubular pore, which leads to the formation of monodisperse nanowires. In this report, we employ a mixture of Pt and Au precursors to produce alloy-type nanowires with compositions that correspond to the relative concentrations of the precursors used in the reaction.

The size and morphology of the nanowires were characterized by scanning electron microscopy (SEM). Figure 1A,B shows representative images of the alloy nanowires consisting of 10 and 90% Au, respectively. The SEM data confirm that the as-synthesized samples consist of monodisperse nanowires with an average diameter of 80 ± 15 nm and aspect ratios of 50−100. SEM data collected from samples with compositions ranging from 0 to 90% Au reveal that the size and morphology of the resulting nanowires remain consistent regardless of the composition. The ability of the template-based method to produce nanowires of the same size and morphology regardless of composition is important and allows us to focus on the influence of composition on electrocatalytic performance.

Energy-dispersive X-ray spectroscopy (EDX) was employed to measure the relative Pt and Au content in the nanowires as a function of the ratio of Pt and Au content in the precursor solution (Figure 1C). Increasing the Au content in the precursor solution results in a corresponding increase in the Au content within the resulting nanowire. Unlike in prior reports,[44,62] the co-reduction of Pt and Au results in a nonlinear relationship between the composition of the precursor solution and the composition of the resulting nanowires. For example, a precursor solution containing 10% Au results in nanowires with a composition of 40% Au. The increased Au content in the nanowires is likely due to the lower number of electrons required to reduce Au^{3+} in $HAuCl_4$ relative to Pt^{4+} in H_2PtCl_6 and the higher reduction potential of Au. Regardless, nanowires with compositions ranging from 5 to 90% Au can be predictably and reproducibly prepared utilizing the data shown in Figure 1D and Table S1. To demonstrate the reproducibility of the synthesis, each of the data given in Figure 1C is shown as an average with an accompanying standard deviation from multiple syntheses.

The composition of the nanowires and their crystalline structure were examined by powder X-ray diffraction (XRD). Representative XRD patterns are shown in Figure 1D for nanowire compositions ranging from 0 to 100% Au. The XRD pattern of the pure Pt and pure Au nanowires could be indexed to the (111), (200), (220), and (311) reflections of face-centered cubic Pt and Au, respectively. As the Au content is increased in the alloy nanowires, the XRD peaks shift uniformly toward the peak positions of pure Au, which is expected for the $Pt_{1-x}Au_x$ alloy. In addition, we do not observe peaks that can be assigned to either pure Pt or Au in the alloy nanowires, suggesting that the wires do not consist of a physical mixture of the pure Pt and Au phases. Utilizing the positions of the XRD peak, a plot of the lattice parameter as a

https://doi.org/10.1021/acsami.1c17244
ACS Appl. Mater. Interfaces 2021, 13, 59892−59903

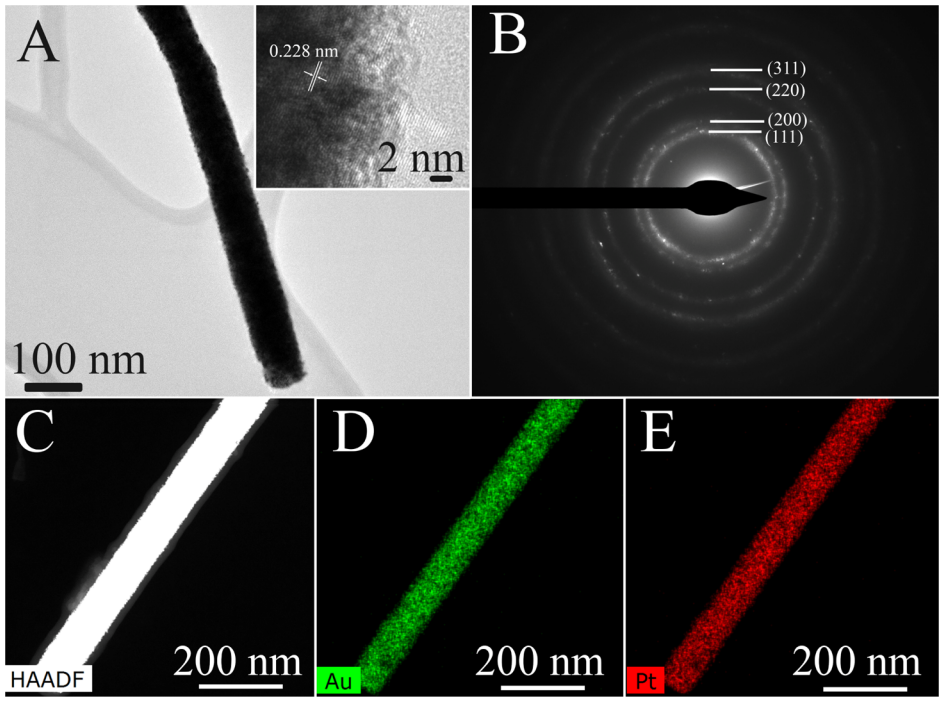

Figure 2. TEM (A) images of a representative, individual $Pt_{1-x}Au_x$ nanowire containing 35% Au. The inset displays a high-resolution TEM image of edge of the nanowire. A selected area electron diffraction (B) pattern collected from the wire depicted in the TEM image. A HAADF scanning TEM image is also shown (C) with EDX maps of Au (D) and Pt (E).

function of the EDX nanowire composition (Figure S2A) yields a linear trend (R^2 = 0.996) consistent with an alloy-type crystal structure. Nanowire compositions calculated using Vegard's law and the calculated lattice parameters (Figure S2B) closely match the corresponding EDX measurements with a mean absolute difference of 2.3% between these measurements.

In order to characterize the crystallinity and uniformity of the individual nanowires, we obtained high-resolution transmission electron microscopy (HRTEM) and high angle annular dark field (HAADF) images from an alloy nanowire consisting of 35% gold. The HRTEM image shown in Figure 2A depicts a representative nanowire, and high magnification images collected at the edge of the wire reveal that it consists of interconnected crystallites. The lattice fringes observed in the image have an interplanar spacing of 0.228 nm, which is consistent with the lattice spacing of the FCC $Pt_{1-x}Au_x$ alloy. The selected area electron diffraction pattern (Figure 2B) displays concentric diffraction rings that can be indexed to the (111), (200), (220), and (311) reflections calculated for the FCC structure of the alloy. The HAADF image (Figure 2C) reveals that the nanowire has a uniform contrast along both axes of the wire, suggesting that there is a homogenous distribution of Pt and Au. We also obtained EDX maps of Au and Pt shown in Figure 2D,E, respectively, and the uniformity of the Pt and Au signals over the entire nanowire further highlights that the nanowire maintains a uniform composition over its entire structure.

XPS was employed to examine the electronic properties and surface composition of the nanowires. High-resolution spectra of the Pt and Au 4f regions are shown in Figure S3, and the peaks can be assigned to the $4f_{5/2}$ and $4f_{7/2}$ transitions for both elements. The composition does not measurably affect the position of the Au peaks, which is consistent with prior results.[63] By contrast, increasing the Au content from 15 to 90% results in a 0.5 eV shift of the Pt 4f peaks to lower binding energy (see Table S2). The shift to lower binding energies is attributed to an upshift of the Pt d-band that arises from an electronic effect of the Au atoms in the alloy.[63] Prior theoretical work has shown that upshifts in the Pt d-band strengthen interactions with adsorbates such as oxygen, CO, and SOMs.[64−66] An increase in the binding strength of oxygen can facilitate SOM oxidation because Pt−OH* and Pt−O* species form at lower potentials and can facilitate CO oxidation. However, an upshift in the Pt d-band can also increase the binding strength of partially oxidized intermediates and CO thereby increasing poisoning effects.

In terms of composition, the XPS data reveal that, under vacuum, the surface composition of the nanowires is consistent with the nominal composition determined by EDX and XRD. Thus, the synthetic method does not result in a significant segregation of one element to the surface of the nanowire in air or in vacuum. Although no significant surface segregation was observed under vacuum, electrochemical measurements are performed under acidic, aqueous conditions with an applied potential. In addition, the adsorption of hydrogen and oxygen species during cyclic voltammetry (CV) can selectively draw electrochemically active atoms to the surface, leading to an electrochemical segregation process.[67,68]

To explore the possible surface distributions of a bimetallic PtAu alloy nanowire of a given nominal composition, Metropolis Monte Carlo simulations were performed using 900-atom nanoslabs of varying ratios of Pt and Au. The nanoslab geometry allows us to study the relevant bulk and surface partitioning of the species, while being more computationally tractable than the full 80 nm diameter nanowire. Simulations were performed both in vacuum and in the presence of oxygen adsorbates to reflect typical electrochemical conditions employed in the oxidation of SOMs. The initial Pt and Au locations were assigned randomly, and the equilibrium

https://doi.org/10.1021/acsami.1c17244
ACS Appl. Mater. Interfaces 2021, 13, 59892−59903

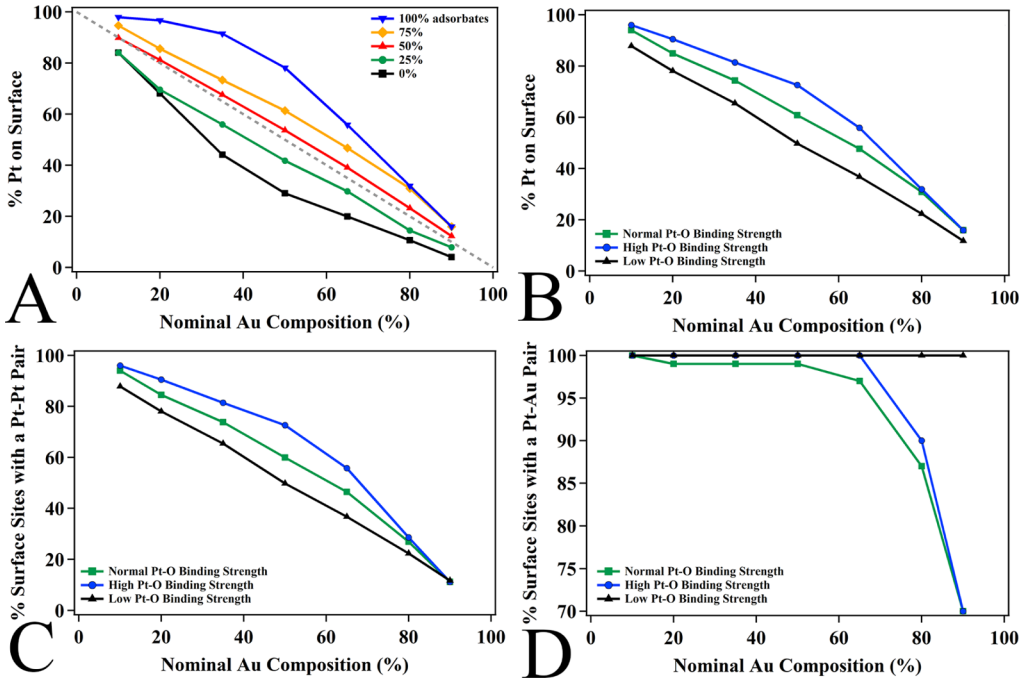

Figure 3. (A) Percentage of surface sites occupied by platinum atoms (% Pt on surface) as a function of the nominal Au composition with various levels of oxygen adsorbate coverage calculated with the Pt−O binding energy for bulk platinum (415 kJ/mol). The gray dashed line denotes a 1:1 relationship between the surface Pt content and nominal Pt content. (B) Influence of Pt−O binding strength on % Pt on the surface as a function of the nominal Au composition with 75% adsorbate coverage. Influence of Pt−O binding strength on the percentage of surface sites with at least (C) one Pt−Pt pair and (D) one Pt−Au pair as a function of the nominal Au composition with 75% adsorbate coverage. High and low Pt−O binding strengths represent either a 25% increase (515 kJ/mol) or a 25% decrease (315 kJ/mol) of the Pt−O binding strength relative to the Pt−O binding strength on bulk Pt.

distribution was found by performing parallel tempering Metropolis Monte Carlo calculations using the metal alloy nanoparticle cohesive bond energy model of Yan et al.,[69] which we extended to include surface adsorbates. This intentionally minimalistic model relies solely on the bulk cohesive energy and pairwise bond dissociation energies and neglects surface reconstruction, strain effects, or collective interactions. Our goal is to understand the qualitative physical underpinnings of the system, without aiming for quantitative precision. Statistics were collected on the equilibrium averages for energy, numbers of atoms of each element in the bulk and on the surface, and number of surface Pt atoms paired with other surface Pt and Au atoms. A complete description of the computational methods can be found in the Supporting Information, and the Python 3.70 code is available on Github.[70]

The average fraction of surface sites occupied by Pt atoms for each nominal composition tested and each adsorbate coverage level utilizing the Pt−O binding energy for bulk Pt (415 kJ/mol) is shown in Figure 3A. The influence of the oxidizing environment is modeled by varying the amount of the oxygen adsorbate on the surface. We first consider 0% adsorbate coverage levels to simulate the slabs in vacuum (black line). The fraction of surface sites occupied by Pt atoms is less than the nominal fraction of Pt atoms in the slab as a whole, indicating that the surface is enriched in Au. This is consistent with the more negative cohesive energy of Pt than Au, so in the absence of other factors, the total energy is minimized when Pt is more coordinated, which thermodynamically favors an Au-enriched surface under these conditions. However, this is not observed in our XPS measurements in vacuum. This is likely due to the synthetic conditions and the use of the strong reducing agent sodium borohydride. Rapid reduction of the precursors is expected to lead to a uniform distribution favored by kinetics rather than a gold enriched surface favored by thermodynamics.

During the CV experiments, adsorption of oxygen species causes electrochemically active atoms to segregate to the surface. Our model allows us to study these trends by adjusting the oxygen adsorbate coverage, depicted in Figure 3A. As the oxygen adsorbate coverage level increases, the fraction of surface sites occupied by Pt atoms becomes greater than the nominal fraction of Pt atoms overall, and the surface becomes increasingly enriched in Pt. This results from the strong Pt−O binding affinity as compared with the Au−O binding affinity. Because Pt binds more strongly to oxygen than does Au, the overall structure is stabilized when Pt atoms are on the surface and able to adsorb oxygen. Numerical values for these parameters taken from published *ab initio* calculations are included in Table S3. Visual depictions of nanoslabs generated at different points throughout the simulations (Figure S5) demonstrate that as the adsorbate coverage level increases, Pt atoms on the surface preferentially occupy undercoordinated edge and corner sites.

The experimental oxidizing environment is complicated and involves many species that bind to the surface in different ways. We explore the sensitivity to these variations by treating the Pt−O binding energy as a tunable parameter describing the typical adsorption event and investigated the influence of the oxygen binding energy on the surface composition. In Figure 3B, we plot the average percentage of surface sites occupied by Pt atoms as a function of the nominal Au content, with different Pt−O binding energies. We also plot the percentage of surface sites with at least one Pt−Pt pair (Figure 3C) and at least one Pt−Au pair (Figure 3D) as a function of the nominal

https://doi.org/10.1021/acsami.1c17244
ACS Appl. Mater. Interfaces 2021, 13, 59892−59903

Au content with higher (515 kJ/mol) and lower oxygen (315 kJ/mol) binding strengths, relative to the oxygen binding strength on pure Pt. For these calculations, we utilize an oxygen coverage level of 75%, which approximates the relative surface coverage of oxygen species observed in the CV results discussed in the next paragraph. As expected, increasing the binding energy of oxygen by 25% beyond that of the binding energy of oxygen on bulk Pt leads to a higher degree of Pt enrichment at the surface and a higher number of Pt−Pt pair sites relative to the bulk distribution. Figure 3D depicts the percentage of Pt−Au sites as a function of nanowire composition, and we find that essentially 100% of the surface gold atoms has a neighboring platinum atom until a nominal gold composition of 75% is reached. These results suggest that surface gold atoms do not tend to form clusters (i.e., forming predominantly Au−Au sites) but rather disperse uniformly into the platinum-enriched surface (i.e., forming predominantly Pt−Au sites). Thus, relatively low levels of the gold content (<50%) into the nanowire leads to a significant increase in Pt−Au sites but has a comparatively small effect of reducing Pt−Pt sites. In addition, the increased binding energy of oxygen that results from the Au content in $Pt_{1-x}Au_x$ alloys leads to several effects that can influence SOM oxidation performance. Increasing the oxygen binding strength leads to higher Pt−Pt pair site density, which favors the indirect pathway rather than the more efficient "CO-free" direct pathway. However, increasing the oxygen binding energy also leads to higher coverages of adsorbates such as oxygen and CO, which can both influence the mechanism of SOM oxidation.

The electrochemical properties of the $Pt_{1-x}Au_x$ nanowires were examined by CV performed in aqueous 0.1 M perchloric acid, and the results are shown in Figure 4. The pure Pt nanowires display hydrogen adsorption (0−0.4 V) and the oxide (0.6−1.0 V) regions that are characteristic of nanostructured Pt catalysts.[71] Elemental Au does not undergo either hydrogen adsorption or surface oxidation within the potential window for Pt CV. Thus, increasing the Au content in the alloy nanowires results in a proportional suppression of both the hydrogen adsorption and oxide features, which is consistent with Au atoms replacing Pt atoms on the catalyst surface. For example, in a sample of nanowires consisting of 69% gold, the hydrogen adsorption charge was suppressed by 73% in comparison with a sample of pure platinum nanowires with the same mass loading. In addition, the position of the oxide reduction peak shifts from 827 to 789 mV, as the Au content is increased from 0 to 50%. The 40 mV shift in the oxide peak position to lower potentials suggests that the increase in the Au content results in a stronger interaction with oxygen adsorbates. This is consistent with the upshift of the Pt d-band observed in the XPS results.

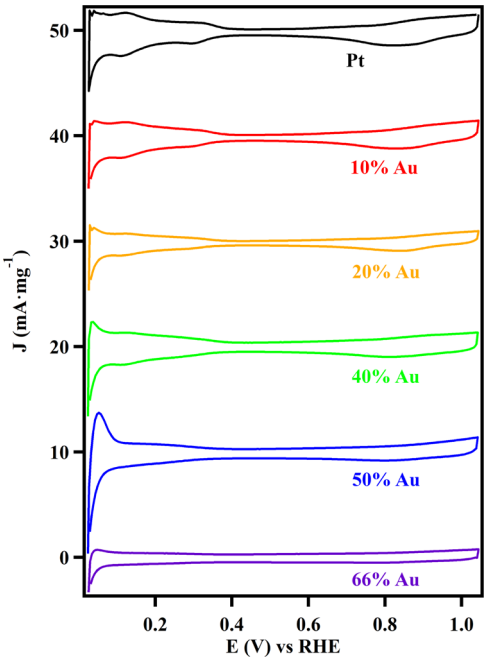

Figure 4. Cyclic voltammograms obtained in 0.1 M $HClO_4$ at a scan rate of 20 mV s^{-1} of $Pt_{1-x}Au_x$ nanowires with the gold content ranging from 0 to 66%.

To examine the influence of composition and Pt−Pt pair site density on the electrocatalytic properties of the $Pt_{1-x}Au_x$ nanowires, we evaluated their performance as methanol oxidation catalysts. The methanol oxidation reaction (MOR) activity was determined from linear sweep voltammograms (LSVs) obtained in 0.1 M perchloric acid containing 0.1 M methanol (Figure 5A). The current density was normalized to the Pt surface area determined from integration of the hydrogen adsorption region to calculate the specific activity. As Au is inactive toward methanol oxidation, the specific activity enables us to examine the intrinsic performance of the Pt active sites on the catalyst surface. The LSVs indicate that increasing the Au content results in a significant enhancement in MOR specific activity over the entire onset region relative to the pure Pt nanowire. To compare performance as a function of composition, the specific activities at 0.7 V were plotted as a function of nanowire composition (Figure 5B). Increasing the Au content from 0 to 40% doubles the specific MOR activity. However, increasing the Au content beyond 40% only increases the activity by an additional 10% achieving a peak activity of 0.50 mA cm^{-2} in the 60% Au sample.

In order to confirm that the electrochemical measurements did not significantly influence the structure of the nanowires, we characterized the morphology and composition of the nanowires before and after a durability test. We performed chronoamperometry at 0.7 V (Figure S7B) to simulate 2 h of catalytic operation. SEM images obtained before and after the durability test (Figure S6) reveal that the size and morphology of the nanowires are retained. EDX measurements also confirm that the overall composition of the nanowires is essentially identical before (37 ± 1% Au) and after (34 ± 2% Au) the durability test. Cyclic voltammograms (Figure S7A) were collected before and after the durability and were also essentially identical in both the hydrogen adsorption and oxide regions, suggesting that the surface structure of the nanowires remains the same.

To investigate the origin of the enhanced MOR performance in the $Pt_{1-x}Au_x$ nanowire, we investigated their activity toward the oxidation of formic acid and CO. CO is a key intermediate that is formed in the indirect pathway. The indirect pathway is expected for pure platinum and platinum-enriched alloy catalysts because of the high density of Pt active sites on the surface. In these catalysts, Pt−Pt pair sites facilitate the dehydrogenation of methanol via a rapid multistep process commonly referred to as α-dehydrogenation, resulting in the formation of an adsorbed CO intermediate at low overpotentials. The complete oxidation of CO to CO_2 is delayed to higher potentials because CO oxidation requires the presence

https://doi.org/10.1021/acsami.1c17244
ACS Appl. Mater. Interfaces 2021, 13, 59892−59903

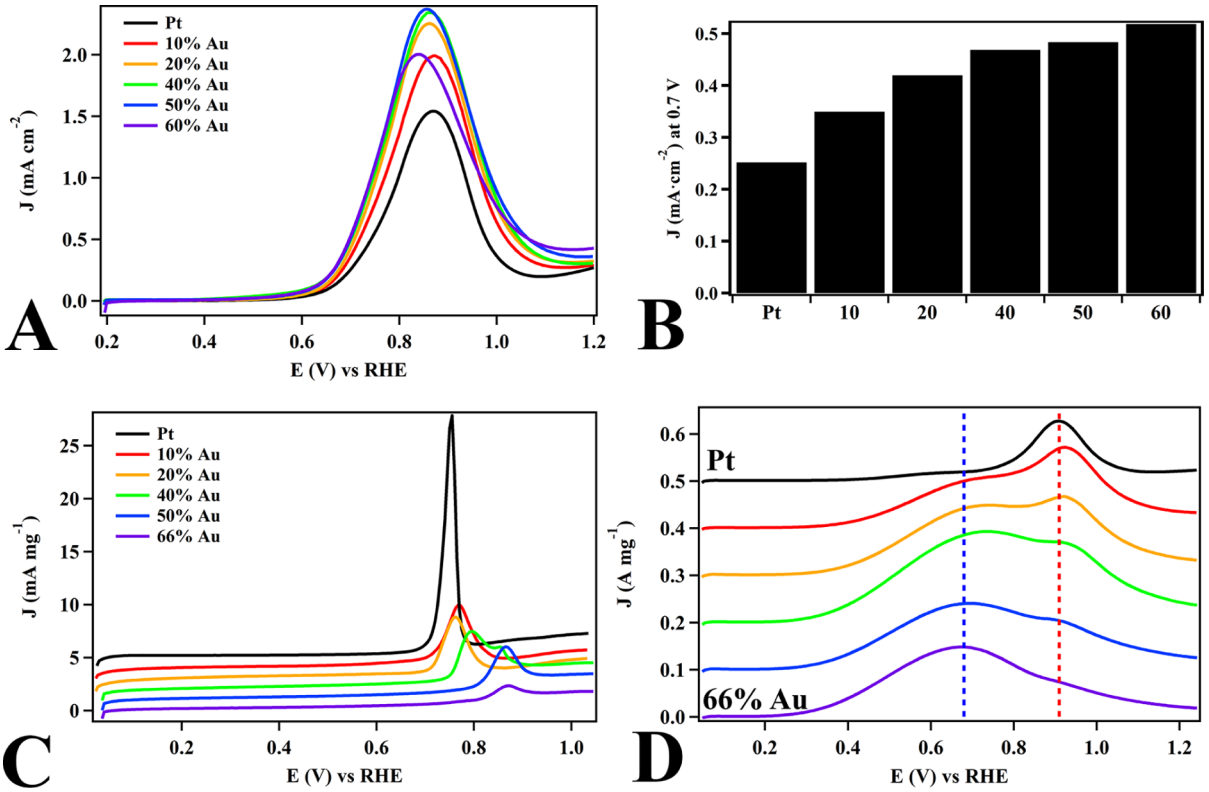

Figure 5. LSVs (A) of $Pt_{1-x}Au_x$ nanowires in 0.1 M methanol/0.1 M $HClO_4$ at a scan rate of 20 mV s^{-1}. A plot of the specific activities measured at 0.7 V as a function of the $Pt_{1-x}Au_x$ nanowire composition (B). CO stripping voltammograms (C) and LSVs in 0.1 M formic acid (D) obtained at 20 mV s^{-1} in the 0.1 M $HClO_4$ electrolyte.

of adsorbed oxygen species, which do not form on Pt at potentials below 0.5−0.6 V. CO is the primary intermediate in the indirect oxidation pathway of methanol, and thus, the performance of catalysts that operate via an indirect pathway will strongly depend on CO oxidation performance.

To determine the relative onset for CO activation and oxidation, CO stripping voltammograms (Figure 5C) were obtained after allowing the catalysts to fully adsorb CO from a CO saturated solution. The addition of Au results in a large positive shift of the CO stripping peak from 757 to 870 mV, as the Au content is increased from 0 to 66%. An upshift in the CO stripping peak suggests that the added Au content decreases the effectiveness of the alloy nanowire toward CO oxidation. Our experimental results are consistent with our XPS results and with computational results,[30] which indicate that alloying platinum and gold results in a significant increase in the binding strength of CO to the surface of the alloy. In this case, the increase in the binding energy of CO leads to a decrease of CO oxidation performance, even though the binding strength of oxygen was also increased. Thus, these results collectively indicate that the increase in MOR performance cannot be explained by an increase in the CO oxidation performance as a result of the gold's electronic effects.

Because Au does not increase CO oxidation performance, a plausible explanation is that its presence on the surface favors a direct pathway for the oxidation of methanol rather than the indirect pathway. In the direct pathway, methanol rapidly reacts with adsorbed oxygen species to form a formic acid intermediate. In a subsequent step, the formic acid is then deprotonated in the rate-limiting step to form CO_2. Thus, the performance of catalysts that proceed via the direct pathway will depend strongly on the ability of the catalyst to oxidize formic acid to CO_2 at low overpotentials. Formic acid can therefore be used as an electrochemical probe to determine if methanol is oxidized via a direct or indirect pathway.[32,72] Catalysts that favor CO formation in SOM oxidation (indirect pathway) will also favor the dehydrogenation of formic acid to CO. The production of CO requires a higher overpotential to achieve complete oxidation to CO_2, and this produces a distinct oxidation wave at 0.9 V in the formic acid LSV. On the other hand, catalysts that favor non-CO pathways (direct mechanism) oxidize formic acid at lower overpotentials without producing a CO intermediate and produce a characteristic oxidation wave at 0.6 V.

To investigate the influence of composition on the oxidation of formic acid, we obtained LSVs in 0.1 M solution of formic acid. The LSVs reveal that increasing the Au content suppresses the peak associated with the indirect pathway and the emergence of the peak associated with the direct pathway, suggesting a uniform transition from the indirect to the direct pathway. The MOR activities and formic acid data suggest that the transition to a direct mechanism occurs within the first 40−50% of the added Au content, with concomitant increases in MOR activity. However, our computational results shown in Figure 3B,C suggest that the decrease in the density of Pt atoms and Pt−Pt pair is relatively shallow, as the Au content is increased to 50%. At 50% Au content and 75% adsorbate coverage, our calculations predict that 65−80% of the surface atoms are platinum and a large fraction (60−75%) of the Pt−Pt pair sites remain at the surface. Thus, the transition to a CO

https://doi.org/10.1021/acsami.1c17244
ACS Appl. Mater. Interfaces 2021, 13, 59892−59903

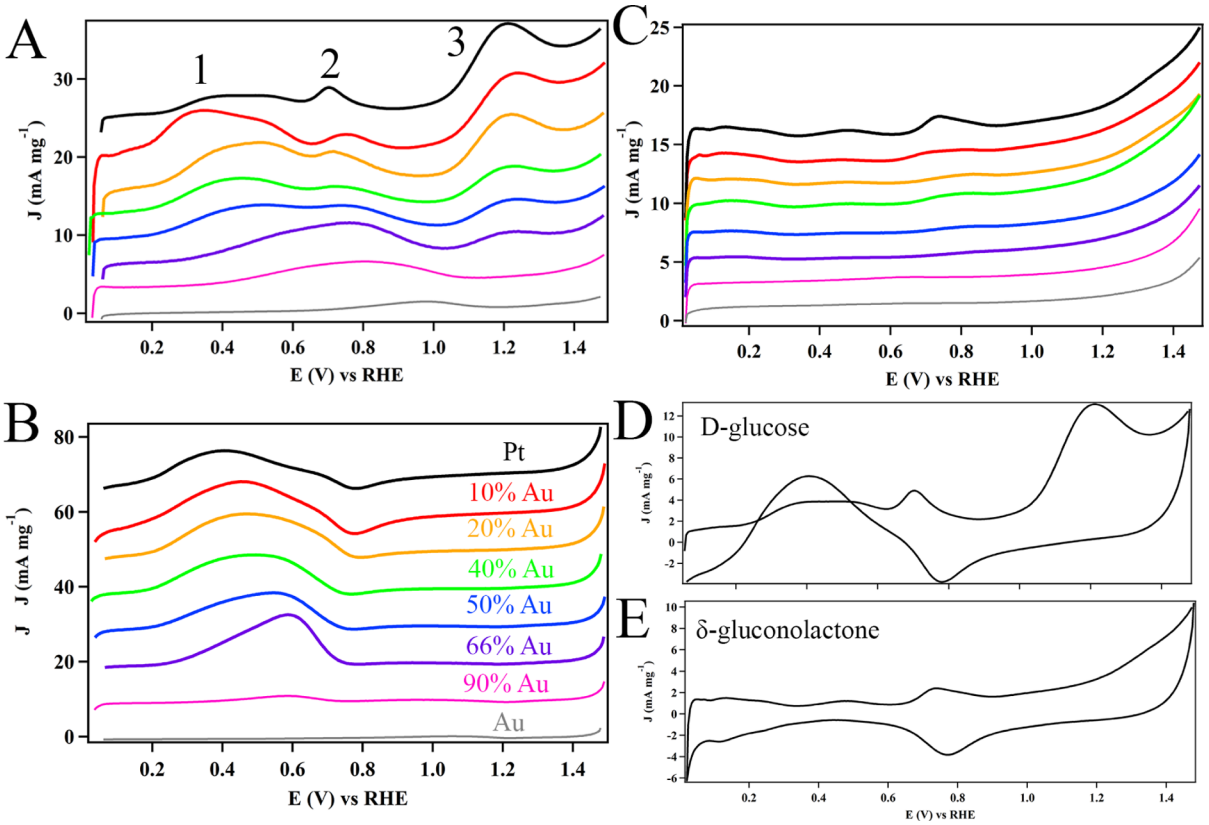

Figure 6. CV data of $Pt_{1-x}Au_x$ NWs in 0.1 M D-glucose/0.1 M perchloric acid in the anodic direction (A) and the cathodic direction (B). The numbers denote the three main peaks in anodic sweep. LSVs of $Pt_{1-x}Au_x$ NWs in 0.1 M *δ*-gluconolactone/0.1 M perchloric acid (C). Cyclic voltammograms of Pt nanowires in 0.1 M D-glucose (D) and 0.1 M *δ*-gluconolactone (E).

free pathway cannot be explained by the decrease in the density of Pt−Pt pair sites alone.

Zhang and co-workers utilized density functional theory (DFT) calculations to simulate the non-CO pathway of methanol oxidation on stoichiometric PtAu(111) alloy surfaces.[30] In the non-CO pathway, methanol is adsorbed on the surface of the alloy and rapidly reacts with adsorbed OH to form an adsorbed HCOOH intermediate. A bridge bond between the HCOOH and adjacent Pt and Au sites stabilizes the HCOOH intermediate and facilitates its rate-limiting deprotonation in this pathway. DFT calculations of methanol oxidation on Pt_2Au (111) and $PtAu_2$ (111) surfaces by Gormley and Berger found that Pt−Au sites raise the transition state for CO migration in the CO-pathway and lower the rate-determining step of the non-CO pathway.[73] This is consistent with the electrochemical results, which demonstrate that the transition to a non-CO pathway occurs within the first 50% of the added Au content. The Monte Carlo results shown in Figure 3D indicate that for 0−50% added gold, essentially all of the surface atoms have at least one neighbor of the other element. Thus, these results collectively suggest that the presence of Pt−Au pair sites may be more significant in defining the oxidation pathway than Pt−Pt pair site density. The practical significance is that CO poisoning can be mitigated by adding a relatively small fraction of Au atoms (~25%) to the surface. Yet, the preference for Pt to sit on the surface (Figure 3A) under operating conditions does not drastically reduce the number of Pt−Pt pair sites on the surface (Figure 3C), which are necessary for initial binding of formic acid during the non-CO pathway.[73]

Collectively, the MOR results indicate that alloying Pt with Au can lead to a significant composition-dependent enhancement in SOM oxidation performance and can shift the oxidation toward a CO-free pathway. However, the oxidation of methanol involves only a single carbon atom. On the other hand, the oxidation of more complex SOM such as D-glucose gives rise to multiple oxidations involving the formation of partially oxidized intermediates including CO. The cyclic voltammogram of the Pt nanowires in 0.1 D-glucose/0.1 M perchloric acid shown in Figure 6D is consistent with prior results obtained from Pt (100) single crystal and nanostructure Pt electrodes.[59,60] The first oxidation wave (0.2−0.4 V, peak 1) is assigned to the oxidation of the hemiacetal hydrogen on C1 leading to a gluconolactone intermediate. The second peak (0.7−0.9 V, peak 2) is attributed to the oxidation of the carbon backbone of glucose and gluconolactone present in the double layer, leading to the formation of a range of oxidized carbon species including CO and CO_2. The final peak (1.0−1.2 V, peak 3) is also attributed to the oxidation of the backbone, leading to the formation of CO and CO_2. Because this oxidation occurs in the potential window where the surface of Pt is oxidized, it is believed that this high potential oxidation may be catalyzed by adsorbed oxygen species. The broad peak in the cathodic sweep occurs within the same potential window as peak 1 in the anodic wave and coincides with hydrogen adsorption. Although this peak has not been widely investigated in prior work, it is thought to be associated with the oxidation of the hemiacetal hydrogen facilitated by the onset of hydrogen adsorption.[45,47]

https://doi.org/10.1021/acsami.1c17244
ACS Appl. Mater. Interfaces 2021, 13, 59892−59903

Based on our MOR results, the presence of Pt−Au sites and the density of Pt−Pt pair sites play important roles in determining the mechanism of SOM oxidation. The oxidation of glucose gives rise to oxidation steps that do not involve CO production (peak 1) and to oxidation steps that do involve CO production (peaks 2 and 3). Thus, tuning the composition and the Pt−Pt and Pt−Au pair site density may provide a pathway for suppressing oxidation steps that lead to CO production. Suppressing CO formation in glucose oxidation has important implications for both fuel cell and sensor applications because the buildup of partially oxidized intermediates reduces oxidation activity and lowers glucose sensitivity. To investigate the role of composition and Pt−Pt pair site density on glucose oxidation, we collected CV data of our $Pt_{1-x}Au_x$ nanowires in solutions containing glucose, and the results are summarized in Figure 6A,B.

In the anodic sweep (Figure 6A), the oxidation waves change significantly with the increasing Au content. Notably, the intensity of peak 3 decreases, as the Au content is increased, and is completely suppressed, as the Au content reaches 90%. The analysis of the oxidation waves at lower potentials is more complex because peaks 1 and 2 overlap. As the Au content increases from 0 to 50%, peak 1 shifts to higher potentials. This is consistent with the CV data for pure Au, which has a single oxidation peak assigned to the oxidation of hemiacetal hydrogen located between 0.9 and 1.0 V. It is therefore not surprising that the position of peak 1 shifts toward higher potentials, as the Au content increases. The position of this second peak remains relatively constant, and intensity decreases as the Au content is increased to 50%. However, above 50% Au content, peaks 1 and 2 merge into a single peak, which shifts to higher potential, as the Au content increases to 90%. Thus, it is difficult to determine if peak 2 is completely suppressed above 50% or if the oxidation of the backbone (peak 2) continues alongside the oxidation of hemiacetal hydrogen, as peak 1 shifts to higher potential.

To elucidate the influence of composition on peak 2, we obtained CV data in 0.1 M δ-gluconolactone (Figure 6C). In gluconolactone, the hemiacetal hydrogen at C1 in glucose is oxidized and this is the major product associated with the oxidation wave at peak 1. This isolates the influence of composition on the oxidation of the gluconolactone backbone (peak 2), as peak 1 will not be present in the CV. The CV of gluconolactone oxidation on pure Pt (Figure 6E) displays a single oxidation wave in the region of peak 2. A small oxidation wave is observed in the region of peak 1 although it is dramatically suppressed relative to glucose oxidation CV. Figure 6C depicts the CVs of $Pt_{1-x}Au_x$ nanowires in gluconolactone. As the Au content is increased, the intensity of peak 2 decreases and is entirely suppressed, as the Au content reaches 50%. Thus, this confirms that increases in the Au content result in a shift of peak 1 to higher potentials that is accompanied by a complete suppression of peak 2.

Collectively, the data shown in Figure 6A,C suggest that the peaks associated with CO formation (peaks 2 and 3) can be selectively suppressed within the first 40−50% of the added Au content in a similar fashion to the MOR results. This provides further evidence that the presence of Pt−Au sites may be more significant in determining the mechanism of SOM oxidation as opposed to Pt−Pt pair site density with PtAu alloys. Although additional work such as *in situ* infrared spectroscopy is necessary, these results also provide evidence that Au sites may play an important role in the adsorption and stabilization of partially oxidized intermediates in the oxidation of glucose. Further work is underway to characterize the adsorption of glucose on PtAu alloys that is beyond the scope of this work. Additional discussion of the electrochemical results including the cathodic sweep shown in Figure 6B can be found in the Supporting Information.

In addition to characterizing the influence of composition on the mechanism of glucose oxidation, we also characterized the performance of the PtAu nanowires for the electrochemical detection of glucose. The sensitivity and limit of detection results as a function of composition are summarized in Table 1,

Table 1. Glucose Sensitivity and Limit of Detection Data for $Pt_{1-x}Au_x$ Nanowires[a]

catalyst % Au	sensitivity (1−5 mM) μA cm^{-2} mM^{-1}	sensitivity (5−18 mM) μA cm^{-2} mM^{-1}	limit of detection μM
0	12.6	24.7	20
10	14.2	26.7	10
20	9.7	19	10
40	7.57	18.6	0.5
50	5.97	14.8	<0.5
66	0.84	1.09	<0.5

[a]The sensitivity measurements were obtained at 0.5 V.

and typical results for the PtAu alloy nanowires are shown in Figure S8. In terms of sensitivity, we observe two linear regions in the physiological glucose concentration range spanning a low concentration regime (1−7 mM) and a high concentration regime (5−18 mM). The highest sensitivity of 26.7 μA cm^{-2} mM^{-1} was achieved at 10% Au, which was approximately 10% higher than the sensitivity of pure Pt. As the Au content is increased from 10 to 50%, the sensitivity decreases by 45% to 14.8 μA cm^{-2} mM^{-1}. Beyond 50%, the sensitivity decreases rapidly to 1.09 μA cm^{-2} mM^{-1} representing a 95% reduction, as the Au content is increased to 66%. The rapid decline in sensitivity when the Au content is increased above 50% suggests that a high Pt site density is necessary to achieve high sensitivity in the physiological concentration range. In this concentration range, the concentration of glucose is significantly lower than the concentration utilized for LSV (0.1 M). Thus, oxidation performance likely becomes dependent on the catalysts' ability to absorb glucose at low concentration, which is facilitated by the strong adsorption on Pt sites. In contrast with the sensitivity results, the limit of detection significantly increases, as the Au content is increased. This is consistent with prior results, which demonstrate that nanostructured Au catalysts have lower limits of detection than Pt-based catalysts.[47]

CONCLUSIONS

The electrochemical oxidation of SOMs such as methanol and glucose is a critical process and has relevant applications in fuel cells and sensors. A key challenge in SOM oxidation is the formation of CO and other partially oxidized intermediates, which poison the catalyst surface and decrease long-term performance and cost-effectiveness. A promising pathway for overcoming this challenge is to tune the surface structure and properties of catalysts to selectively oxidize SOMs via "direct" pathways that do not form CO as a primary intermediate. CO formation on Pt-based catalysts is attributed to the presence of Pt−Pt pair sites, which facilitate rapid dehydrogenation and

https://doi.org/10.1021/acsami.1c17244
ACS Appl. Mater. Interfaces 2021, 13, 59892−59903

stabilize CO intermediates. Thus, the focus of prior work has been to reduce or eliminate Pt−Pt pair sites by preparing a wide range of alloy-type nanostructures.

In this report, we utilize an ambient, template-based approach to prepare PtAu alloy nanowires with tunable compositions. XPS measurements reveal that the surface composition matches that of the bulk composition after synthesis. Monte Carlo simulations of the surface structure of PtAu alloys with varying coverage of oxygen adsorbates and varying degrees of oxygen adsorption strength reveal that oxygen adsorption under electrochemical conditions enriches the surface with Pt and a large fraction of Pt−Pt sites remain on the surface even with the Au content of up to 50%. Electrochemical properties and the catalytic performance measurements of the PtAu nanowires for the oxidation of methanol and glucose reveal that the mechanistic pathways that produce CO are suppressed by the addition of relatively small quantities of Au (∼10%) and CO formation can be completely suppressed by 50% Au. The suppression of CO formation with small quantities of Au suggests that the presence of Pt−Au pair sites may be more important in determining the mechanism of SOM oxidation rather than Pt−Pt pair site density, in agreement with predictions from previous DFT calculations.

EXPERIMENTAL METHODS

The $Pt_{1-x}Au_x$ alloy nanowires were synthesized using the *U*-tube double diffusion technique.[62,74−76] The *U*-tube double diffusion device (Figure S1) consists of two glass half-cells that are separated by a polycarbonate filter membrane, serving as a template for the growth of nanowires. The precursor solution is prepared by dissolving hexachloroplatinic acid (H_2PtCl_6, Alfa Aesar, 99.9%) and tetrachloroauric acid ($HAuCl_4$, Alfa Aesar, 99.9%) in absolute ethanol to form a solution with a combined metal concentration of 15 mM. The relative concentration of Pt and Au in the precursor solution was optimized to produce alloy nanowires with the Pt content ranging from 90 to 15% (see Table S1). The reducing agent solution was prepared by dissolving sodium borohydride (Alfa Aesar, 98%) in absolute ethanol to form a 5 mM solution. Prior to use, the polycarbonate filter membrane (Whatman, Nucleopore Track Etch, 50 nm nominal pore diameter) was sonicated in absolute ethanol to saturate the pores. In a typical reaction, the *U*-tube device is assembled by clamping the filter membrane between the two half-cells. The precursor and reducing agent solutions are added simultaneously, and the reaction is allowed to proceed for 30 min.

Upon completion of the reaction, the template is rinsed with absolute ethanol to remove residual contaminants and is polished on an Arkansas soft whetstone to remove any metallic material that was formed on the surface of the template. The nanowires are isolated by dissolving the polycarbonate membrane in dichloromethane (Acros Organics, ACS grade), and the nanowires are separated by centrifugation. The nanowires are subsequently washed several times with dichloromethane followed by ethanol to yield the purified alloy nanowires. Catalyst inks of the nanowires were prepared by dispersing the nanowires into absolute ethanol (Fisher Scientific, Optima grade) with a concentration of 2 $mg{\cdot}mL^{-1}$.

N.S. and A.R. contributed equally to this work. N.S., A.R., W.B., K.K., and R.T. synthesized and characterized the PtAu nanowires. A.R., W.B., L.S., and C.K. performed electrochemical measurements. Y.W. and J.Z. collected and analyzed the high-resolution TEM data. N.S. and J.S. performed the computational simulations.

ASSOCIATED CONTENT

Supporting Information

The Supporting Information is available free of charge at https://pubs.acs.org/doi/10.1021/acsami.1c17244.

Additional details of the characterization of the nanowires, electrochemical methods, computational methods, and discussion of the electrochemical results (PDF)

AUTHOR INFORMATION

Corresponding Authors

Joshua Schrier − *Department of Chemistry, Fordham University, Bronx, New York 10458, United States;* orcid.org/0000-0002-2071-1657; Email: jschrier@fordham.edu

Christopher Koenigsmann − *Department of Chemistry, Fordham University, Bronx, New York 10458, United States;* orcid.org/0000-0002-2870-1509; Email: ckoenigsmann@fordham.edu

Authors

Nicole Smina − *Department of Chemistry, Fordham University, Bronx, New York 10458, United States*

Adam Rosen − *Department of Chemistry, Fordham University, Bronx, New York 10458, United States*

Lukasz Sztaberek − *Department of Chemistry, Fordham University, Bronx, New York 10458, United States; Department of Environmental Control Technology, New York City College of Technology, Brooklyn, New York 11201, United States*

William Beatrez − *Department of Chemistry, Fordham University, Bronx, New York 10458, United States*

Kathryn Kingsbury − *Department of Chemistry, Fordham University, Bronx, New York 10458, United States*

Rosario Troia − *Department of Chemistry, Fordham University, Bronx, New York 10458, United States*

Yongchen Wang − *Department of Chemistry, University of Connecticut, Storrs, Connecticut 06269-3060, United States;* orcid.org/0000-0003-0792-2908

Jing Zhao − *Department of Chemistry, University of Connecticut, Storrs, Connecticut 06269-3060, United States;* orcid.org/0000-0002-6882-2196

Complete contact information is available at: https://pubs.acs.org/10.1021/acsami.1c17244

Notes

The authors declare no competing financial interest.

ACKNOWLEDGMENTS

C.K. thanks the Russo Family Foundation for a grant provided for the purchase of the SEM and EDX instruments used in this study. C.K. would also like to thank the Yale University West Campus Materials Characterization Core and Min Lin for the use of their X-ray photoelectron instrument. This project used the computational resources of the MERCURY consortium (http://mercuryconsortium.org/) supported under NSF grant CNS-2018427. N.S., A.R., W.B., and K.K. thank Fordham College at Rose Hill for financial support through undergraduate research grants. N.S. and K.K. would also like to thank the Clare Boothe Luce Foundation for support through the Clare Boothe Luce scholarship. N.S. and J.S. acknowledge support by the Henry Dreyfus Teacher-Scholar Award (TH-14-010) and the National Science Foundation (DMR-1928882).

ABBREVIATIONS

SOM, small organic molecule

CO, carbon monoxide
XRD, X-ray powder diffraction
XPS, X-ray photoelectron spectroscopy
SEM, scanning electron microscopy
HRTEM, high-resolution transmission electron microscopy
HAADF, high angle annular dark field imaging
CV, cyclic voltammetry
LSV, linear sweep voltammetry
MOR, methanol oxidation reaction

REFERENCES

(1) Zhong, C.-J.; Luo, J.; Njoki, P. N.; Mott, D.; Wanjala, B.; Loukrakpam, R.; Lim, S.; Wang, L.; Fang, B.; Xu, Z. Fuel Cell Technology: Nano-Engineered Multimetallic Catalysts. *Energy Environ. Sci.* **2008**, *1*, 454−466.
(2) Chuan-Jian, Z.; Jin, L.; Bin, F.; Bridgid, N. W.; Peter, N. N.; Rameshwori, L.; Jun, Y. Nanostructured Catalysts in Fuel Cells. *Nanotechnology* **2010**, *21*, 062001.
(3) Antolini, E.; Lopes, T.; Gonzalez, E. R. An Overview of Platinum-Based Catalysts as Methanol-Resistant Oxygen Reduction Materials for Direct Methanol Fuel Cells. *J. Alloys Compd.* **2008**, *461*, 253−262.
(4) Antolini, E.; Perez, J. The Renaissance of Unsupported Nanostructured Catalysts for Low-Temperature Fuel Cells: From the Size to the Shape of Metal Nanostructures. *J. Mater. Sci.* **2011**, *46*, 1−23.
(5) Koenigsmann, C.; Scofield, M. E.; Liu, H.; Wong, S. S. Designing Enhanced One-Dimensional Electrocatalysts for the Oxygen Reduction Reaction: Probing Size- and Composition-Dependent Electrocatalytic Behavior in Noble Metal Nanowires. *J. Phys. Chem. Lett.* **2012**, *3*, 3385−3398.
(6) Koenigsmann, C.; Wong, S. S. One-Dimensional Noble Metal Electrocatalysts: A Promising Structural Paradigm for Direct Methanol Fuel Cells. *Energy Environ. Sci.* **2011**, *4*, 1161−1176.
(7) Ramli, Z. A. C.; Kamarudin, S. K. Platinum-Based Catalysts on Various Carbon Supports and Conducting Polymers for Direct Methanol Fuel Cell Applications: A Review. *Nanoscale Res. Lett.* **2018**, *13*, 410.
(8) Antolini, E.; Salgado, J. R. C.; Gonzalez, E. R. The Methanol Oxidation Reaction on Platinum Alloys with the First Row Transition Metals: The Case of Pt-Co and -Ni Alloy Electrocatalysts for DMFCs: A Short Review. *Appl. Catal., B* **2006**, *63*, 137−149.
(9) Aricò, A. S.; Srinivasan, S.; Antonucci, V. DMFCs: From Fundamental Aspects to Technology Development. *Fuel Cells* **2001**, *1*, 133−161.
(10) Chu, D.; Jiang, R. Novel Electrocatalysts for Direct Methanol Fuel Cells. *Solid State Ionics* **2002**, *148*, 591−599.
(11) Cowin, P. I.; Petit, C. T. G.; Lan, R.; Irvine, J. T. S.; Tao, S. Recent Progress in the Development of Anode Materials for Solid Oxide Fuel Cells. *Adv. Energy Mater.* **2011**, *1*, 314−332.
(12) Hamnett, A. Mechanism of Methanol Oxidation. In *Interfacial Electrochemistry: Theory, Experiment and Applications*; Wieckowski, A., Ed.; Marcel Dekker: New York, NY, 1999; Chapter 47, pp 843−879.
(13) Sharma, S.; Pollet, B. G. Support Materials for PEMFC and DMFC Electrocatalysts—a Review. *J. Power Sources* **2012**, *208*, 96−119.
(14) Prabhu, P.; Lee, J.-M. Metallenes as Functional Materials in Electrocatalysis. *Chem. Soc. Rev.* **2021**, *50*, 6700−6719.
(15) Wang, H.; Chen, J.; Lin, Y.; Wang, X.; Li, J.; Li, Y.; Gao, L.; Zhang, L.; Chao, D.; Xiao, X.; Lee, J. M. Electronic Modulation of Non-Van der Waals 2D Electrocatalysts for Efficient Energy Conversion. *Adv. Mater.* **2021**, *33*, 2008422.
(16) Wang, H.; Li, J.; Li, K.; Lin, Y.; Chen, J.; Gao, L.; Nicolosi, V.; Xiao, X.; Lee, J.-M. Transition Metal Nitrides for Electrochemical Energy Applications. *Chem. Soc. Rev.* **2021**, *50*, 1354−1390.
(17) Prabhu, P.; Jose, V.; Lee, J.-M. Design Strategies for Development of TMD-Based Heterostructures in Electrochemical Energy Systems. *Matter* **2020**, *2*, 526−553.
(18) Prabhu, P.; Jose, V.; Lee, J. M. Heterostructured Catalysts for Electrocatalytic and Photocatalytic Carbon Dioxide Reduction. *Adv. Funct. Mater.* **2020**, *30*, 1910768.
(19) Wang, H.; Lee, J.-M. Recent Advances in Structural Engineering of MXene Electrocatalysts. *J. Mater. Chem. A* **2020**, *8*, 10604−10624.
(20) Wasmus, S.; Küver, A. Methanol Oxidation and Direct Methanol Fuel Cells: A Selective Review. *J. Electroanal. Chem.* **1999**, *461*, 14−31.
(21) Kunimatsu, K.; Hanawa, H.; Uchida, H.; Watanabe, M. Role of Adsorbed Species in Methanol Oxidation on Pt Studied by ATR-FTIRAS Combined with Linear Potential Sweep Voltammetry. *J. Electroanal. Chem.* **2009**, *632*, 109−119.
(22) Nonaka, H.; Matsumura, Y. Electrochemical Oxidation of Carbon Monoxide, Methanol, Formic Acid, Ethanol, and Acetic Acid on a Platinum Electrode under Hot Aqueous Conditions. *J. Electroanal. Chem.* **2002**, *520*, 101−110.
(23) Liu, P.; Logadottir, A.; Nørskov, J. K. Modeling the Electro-Oxidation of CO and H_2/CO on Pt, Ru, PtRu and Pt_3Sn. *Electrochim. Acta* **2003**, *48*, 3731−3742.
(24) Liu, F.; Lee, J. Y.; Zhou, W. J. Segmented Pt/Ru, Pt/Ni, and Pt/RuNi Nanorods as Model Bifunctional Catalysts for Methanol Oxidation. *Small* **2006**, *2*, 121−128.
(25) Adzic, R. R.; Wang, J. X. Structure of Active Phases During the Course of Electrocatalytic Reactions. *J. Phys. Chem. B* **2000**, *104*, 869−872.
(26) Feibelman, P. J.; Hammer, B.; Nørskov, J. K.; Wagner, F.; Scheffler, M.; Stumpf, R.; Watwe, R.; Dumesic, J. The CO/Pt(111) Puzzle. *J. Phys. Chem. B* **2000**, *105*, 4018−4025.
(27) Gasteiger, H. A.; Markovic, N.; Ross, P. N.; Cairns, E. J. Methanol Electrooxidation on Well-Characterized Platinum-Ruthenium Bulk Alloys. *J. Phys. Chem.* **1993**, *97*, 12020−12029.
(28) Zheng, Y.; Wan, X.; Cheng, X.; Cheng, K.; Dai, Z.; Liu, Z. Advanced Catalytic Materials for Ethanol Oxidation in Direct Ethanol Fuel Cells. *Catalysts* **2020**, *10*, 166.
(29) Menshikov, V. S.; Novomlinsky, I. N.; Belenov, S. V.; Alekseenko, A. A.; Safronenko, O. I.; Guterman, V. E. Methanol, Ethanol, and Formic Acid Oxidation on New Platinum-Containing Catalysts. *Catalysts* **2021**, *11*, 158.
(30) Zhong, W.; Liu, Y.; Zhang, D. Theoretical Study of Methanol Oxidation on the PtAu(111) Bimetallic Surface: CO Pathway Vs Non-CO Pathway. *J. Phys. Chem. C* **2012**, *116*, 2994−3000.
(31) Yuan, D.; Gong, X.; Wu, R. Decomposition Pathways of Methanol on the PtAu(111) Bimetallic Surface: A First-Principles Study. *J. Chem. Phys.* **2008**, *128*, 064706−64715.
(32) Cui, C.-H.; Li, H.-H.; Cong, H.-P.; Yu, S.-H.; Tao, F. Direct Evidence for Active Site-Dependent Formic Acid Electro-Oxidation by Topmost-Surface Atomic Redistribution in a Ternary PtPdCu Electrocatalyst. *Chem. Commun.* **2012**, *48*, 12062−12064.
(33) Choi, J.-H.; Park, K.-W.; Park, I.-S.; Kim, K.; Lee, J.-S.; Sung, Y.-E. A PtAu Nanoparticle Electrocatalyst for Methanol Electro-Oxidation in Direct Methanol Fuel Cells. *J. Electrochem. Soc.* **2006**, *153*, A1812−A1817.
(34) Luo, J.; Njoki, P. N.; Lin, Y.; Mott, D.; Wang; Zhong, C.-J. Characterization of Carbon-Supported AuPt Nanoparticles for Electrocatalytic Methanol Oxidation Reaction. *Langmuir* **2006**, *22*, 2892−2898.
(35) Mott, D.; Luo, J.; Njoki, P. N.; Lin, Y.; Wang, L.; Zhong, C.-J. Synergistic Activity of Gold-Platinum Alloy Nanoparticle Catalysts. *Catal. Today* **2007**, *122*, 378−385.
(36) Yang, L.; Yang, W.; Cai, Q. Well-Dispersed PtAu Nanoparticles Loaded into Anodic Titania Nanotubes: A High Antipoison and Stable Catalyst System for Methanol Oxidation in Alkaline Media. *J. Phys. Chem. C* **2007**, *111*, 16613−16617.
(37) Yin, M.; Huang, Y.; Liang, L.; Liao, J.; Liu, C.; Xing, W. Inhibiting CO Formation by Adjusting Surface Composition in Ptau Alloys for Methanol Electrooxidation. *Chem. Commun.* **2011**, *47*, 8172−8174.

https://doi.org/10.1021/acsami.1c17244
ACS Appl. Mater. Interfaces 2021, 13, 59892−59903

(38) Zhao, X.; Yin, M.; Ma, L.; Liang, L.; Liu, C.; Liao, J.; Lu, T.; Xing, W. Recent Advances in Catalysts for Direct Methanol Fuel Cells. *Energy Environ. Sci.* **2011**, *4*, 2736−2753.
(39) He, W.; Liu, J.; Qiao, Y.; Zou, Z.; Zhang, X.; Akins, D. L.; Yang, H. Simple Preparation of Pd−Pt Nanoalloy Catalysts for Methanol-Tolerant Oxygen Reduction. *J. Power Sources* **2010**, *195*, 1046−1050.
(40) Lee, C.-L.; Chiou, H.-P. Methanol-Tolerant Pd Nanocubes for Catalyzing Oxygen Reduction Reaction in H_2SO_4 Electrolyte. *Appl. Catal., B* **2012**, *117*−*118*, 204−211.
(41) Lee, C.-L.; Chiou, H.-P.; Wu, S.-C.; Wu, C.-C. Alloy Ratio Effect of Pd/Pt Nanoparticles on Carbon Nanotubes for Catalysing Methanol-Tolerant Oxygen Reduction. *Electrochim. Acta* **2010**, *56*, 687−692.
(42) Wang, W. M.; Li, Z. L.; Zou, Z.; Yang, H.; Feng, S. Carbon-Supported Pd-Pt Alloy Nanoparticles for Methanol Tolerant Oxygen Reduction. *ECS Trans.* **2008**, *16*, 613−619.
(43) Yang, J.; Zhou, W.; Cheng, C. H.; Lee, J. Y.; Liu, Z. Pt-Decorated PdFe Nanoparticles as Methanol-Tolerant Oxygen Reduction Electrocatalyst. *ACS Appl. Mater. Interfaces* **2009**, *2*, 119−126.
(44) Koenigsmann, C.; Wong, S. S. Tailoring Chemical Composition to Achieve Enhanced Methanol Oxidation Reaction and Methanol-Tolerant Oxygen Reduction Reaction Performance in Palladium-Based Nanowire Systems. *ACS Catal.* **2013**, *3*, 2031−2040.
(45) Toghill, K. E.; Compton, R. G. Electrochemical Non-Enzymatic Glucose Sensors: A Perspective and an Evaluation. *Int. J. Electrochem. Sci.* **2010**, *5*, 1246−1301.
(46) Park, S.; Boo, H.; Chung, T. D. Electrochemical Non-Enzymatic Glucose Sensors. *Anal. Chim. Acta* **2006**, *556*, 46−57.
(47) Wang, G.; He, X.; Wang, L.; Gu, A.; Huang, Y.; Fang, B.; Geng, B.; Zhang, X. Non-Enzymatic Electrochemical Sensing of Glucose. *Microchim. Acta* **2013**, *180*, 161−186.
(48) Zhu, C.; Guo, S.; Dong, S. PdM (M = Pt, Au) Bimetallic Alloy Nanowires with Enhanced Electrocatalytic Activity for Electro-Oxidation of Small Molecules. *Adv. Mater.* **2012**, *24*, 2326−2331.
(49) Dai, L.; Mo, S.; Qin, Q.; Zhao, X.; Zheng, N. Carbon Monoxide-Assisted Synthesis of Ultrathin $PtCu_3$ Alloy Wavy Nanowires and Their Enhanced Electrocatalysis. *Small* **2016**, *12*, 1572−1577.
(50) Lin, J.; Tang, D. Glucometer-Based Signal Readout for a Portable Low-Cost Electrochemical Immunoassay Using Branched Platinum Nanowires. *Anal. Methods* **2016**, *8*, 4069−4074.
(51) Gao, G.; Zhang, Z.; Wang, K.; Yuan, Q.; Wang, X. One-Pot Synthesis of Dendritic Pt_3Ni Nanoalloys as Nonenzymatic Electrochemical Biosensors with High Sensitivity and Selectivity for Dopamine Detection. *Nanoscale* **2017**, *9*, 10998−11003.
(52) Wu, W.-P.; Periasamy, A. P.; Lin, G.-L.; Shih, Z.-Y.; Chang, H.-T. Palladium Copper Nanosponges for Electrocatalytic Reduction of Oxygen and Glucose Detection. *J. Mater. Chem. A* **2015**, *3*, 9675−9681.
(53) Vilana, J.; Lorenzo, M.; Gómez, E.; Vallés, E. Electrochemical Deposition of CoNi Micro/Nanostructures as New Materials for Electrochemical Sensing of Glucose. *Mater. Lett.* **2015**, *159*, 154−158.
(54) Li, Y.; Niu, X.; Tang, J.; Lan, M.; Zhao, H. A Comparative Study of Nonenzymatic Electrochemical Glucose Sensors Based on Pt-Pd Nanotube and Nanowire Arrays. *Electrochim. Acta* **2014**, *130*, 1−8.
(55) Cherevko, S.; Chung, C.-H. Gold Nanowire Array Electrode for Non-Enzymatic Voltammetric and Amperometric Glucose Detection. *Sens. Actuators, B* **2009**, *142*, 216−223.
(56) Lu, L.-M.; Zhang, L.; Qu, F.-L.; Lu, H.-X.; Zhang, X.-B.; Wu, Z.-S.; Huan, S.-Y.; Wang, Q.-A.; Shen, G.-L.; Yu, R.-Q. A Nano-Ni Based Ultrasensitive Nonenzymatic Electrochemical Sensor for Glucose: Enhancing Sensitivity through a Nanowire Array Strategy. *Biosens. Bioelectron.* **2009**, *25*, 218−223.
(57) Singh, B.; Laffir, F.; McCormac, T.; Dempsey, E. PtAu/C Based Bimetallic Nanocomposites for Non-Enzymatic Electrochemical Glucose Detection. *Sens. Actuators, B* **2010**, *150*, 80−92.
(58) Kokkindis, G.; Leger, J. M.; Lamy, C. Structural Effects in Electrocatalysis: Oxidation of D-Glucose on Pt (100), (110) and (111) Single Crystal Electrodes and the Effect of UPD Adlayers of Pb, Tl and Bi. *J. Electroanal. Chem.* **1988**, *242*, 221−242.
(59) Popović, K. Đ.; Tripković, A. V.; Adžić, R. R. Oxidation of D-Glucose on Single-Crystal Platinum Electrodes: A Mechanistic Study. *J. Electroanal. Chem.* **1992**, *339*, 227−245.
(60) Popović, K. D.; Marković, N. M.; Tripković, A. V.; Adžić, R. R. Structural Effects in Electrocatalysis: Oxidation of D-Glucose on Single Crystal Platinum Electrodes in Alkaline Solution. *J. Electroanal. Chem.* **1991**, *313*, 181−199.
(61) Popović, K.; Tripković, A.; Marković, N.; Adžić, R. R. Structural Effects in Electrocatalysis: Oxidation of Glucose on Single-Crystal Platinum Electrodes. *J. Electroanal. Chem.* **1990**, *295*, 79−94.
(62) Koenigsmann, C.; Sutter, E.; Adzic, R. R.; Wong, S. S. Size- and Composition-Dependent Enhancement of Electrocatalytic Oxygen Reduction Performance in Ultrathin Palladium-Gold ($Pd_{1-x}Au_x$) Nanowires. *J. Phys. Chem. C* **2012**, *116*, 15297−15306.
(63) Wang, D.; Cui, X.; Xiao, Q.; Hu, Y.; Wang, Z.; Yiu, Y. M.; Sham, T. K. Electronic Behaviour of Au-Pt Alloys and the 4f Binding Energy Shift Anomaly in Au Bimetallics- X-Ray Spectroscopy Studies. *AIP Adv.* **2018**, *8*, 065210.
(64) Kitchin, J. R.; Nørskov, J. K.; Barteau, M. A.; Chen, J. G. Modification of the Surface Electronic and Chemical Properties of Pt(111) by Subsurface 3d Transition Metals. *J. Chem. Phys.* **2004**, *120*, 10240−10246.
(65) Norskov, J. K.; Rossmeisl, J.; Logadottir, A.; Lindqvist, L.; Kitchin, J. R.; Bligaard, T.; Jonsson, H. Origin of the Overpotential for Oxygen Reduction at a Fuel-Cell Cathode. *J. Phys. Chem. B* **2004**, *108*, 17886−17892.
(66) Nørskov, J. K.; Bligaard, T.; Rossmeisl, J.; Christensen, C. H. Towards the Computational Design of Solid Catalysts. *Nat. Chem.* **2009**, *1*, 37−46.
(67) Mayrhofer, K. J. J.; Hartl, K.; Juhart, V.; Arenz, M. Degradation of Carbon-Supported Pt Bimetallic Nanoparticles by Surface Segregation. *J. Am. Chem. Soc.* **2009**, *131*, 16348−16349.
(68) Mayrhofer, K. J. J.; Juhart, V.; Hartl, K.; Hanzlik, M.; Arenz, M. Adsorbate-Induced Surface Segregation for Core−Shell Nanocatalysts. *Angew. Chem., Int. Ed.* **2009**, *48*, 3529−3531.
(69) Yan, Z.; Taylor, M. G.; Mascareno, A.; Mpourmpakis, G. Size-, Shape-, and Composition-Dependent Model for Metal Nanoparticle Stability Prediction. *Nano Lett.* **2018**, *18*, 2696−2704.
(70) Smina, N.; Schrier, J. Alloy Surface Simulator Github Repository. https://github.com/nsmina914/alloy_surface_simulator (accessed on Nov 3, 2021).
(71) Garsany, Y.; Baturina, O. A.; Swider-Lyons, K. E.; Kocha, S. S. Experimental Methods for Quantifying the Activity of Platinum Electrocatalysts for the Oxygen Reduction Reaction. *Anal. Chem.* **2010**, *82*, 6321−6328.
(72) Vidal-Iglesias, F. J.; Solla-Gullón, J.; Herrero, E.; Aldaz, A.; Feliu, J. M. Pd Adatom Decorated (100) Preferentially Oriented Pt Nanoparticles for Formic Acid Electrooxidation. *Angew. Chem., Int. Ed.* **2010**, *49*, 6998−7001.
(73) Gormley, E. L.; Berger, R. F. Binding Maps for the Study and Prediction of Bimetallic Catalyst Surface Reactions: The Case of Methanol Oxidation. *Int. J. Quantum Chem.* **2018**, *118*, No. e25606.
(74) Koenigsmann, C.; Santulli, A. C.; Sutter, E.; Wong, S. S. Ambient, Surfactantless Synthesis, Growth Mechanism, and Size-Dependent Electrocatalytic Behavior of High-Quality, Single Crystalline Palladium Nanowires. *ACS Nano* **2011**, *5*, 7471−7487.
(75) Koenigsmann, C.; Zhou, W.-p.; Adzic, R. R.; Sutter, E.; Wong, S. S. Size-Dependent Enhancement of Electrocatalytic Performance in Relatively Defect-Free, Processed Ultrathin Platinum Nanowires. *Nano Lett.* **2010**, *10*, 2806−2811.
(76) Patete, J. M.; Peng, X.; Koenigsmann, C.; Xu, Y.; Karn, B.; Wong, S. S. Viable Methodologies for the Synthesis of High-Quality Nanostructures. *Green Chem.* **2011**, *13*, 482−519.